ECN

Energy research Centre of the Netherlands

Analysis of fourth-order accurate symmetry-preserving boundary conditions for the incompressible Navier-Stokes equations

B. Sanderse (ECN, CWI)

B. Koren (CWI, Leiden University)

Paper presented at: Fifth European Conference on Computational Fluid Dynamics

ECCOMAS CFD 2010, June 14-17, 2010, Lisbon, Portugal

ECN-M--10-061 June 2010

V European Conference on Computational Fluid Dynamics
ECCOMAS CFD 2010
J. C. F. Pereira and A. Sequeira (Eds)
Lisbon, Portugal,14-17 June 2010

ANALYSIS OF FOURTH-ORDER ACCURATE SYMMETRY-PRESERVING BOUNDARY CONDITIONS FOR THE INCOMPRESSIBLE NAVIER-STOKES EQUATIONS

B. Sanderse*† and B. Koren†‡

*Energy research Centre of the Netherlands (ECN)
Westerduinweg 3, 1755 ZG Petten, the Netherlands
e-mail: sanderse@ecn.nl
† Centrum Wiskunde & Informatica (CWI)
Science Park 123, 1098 XG Amsterdam, the Netherlands
e-mail: barry.koren@cwi.nl
‡ Leiden University, Mathematical Institute
Niels Bohrweg 1, 2333 CA Leiden, the Netherlands

Key words: high-order discretization, symmetry-preserving, mimetic, boundary conditions, error analysis, wind energy

Abstract. *In this paper we investigate symmetry-preserving boundary conditions for a fourth-order symmetry-preserving finite volume method, to able to do accurate turbulence simulations for wind-turbine wake applications. It is found that the use of Dirichlet conditions limits the fourth-order method to (at most) second order. However, on properly chosen non-uniform grids, fourth-order behavior can be displayed on coarse grids, which can make the method attractive for simulations of turbulent flow.*

1 INTRODUCTION

An ongoing challenge in the simulation of wind-turbine wakes and their interaction in wind farms is the accurate representation of turbulence. The origin of turbulence lies both in the atmosphere and in the action of the turbine blades on the flow. Turbulence is a dominating factor in the wake behind a turbine, enhancing mixing with the atmosphere, leading to recovery of the wake deficit, but increasing dynamic blade loading for downstream turbines.

In order to study these effects, the current state-of-the-art is to solve the incompressible Navier-Stokes equations with Large Eddy Simulation (LES) turbulence modeling and an actuator-type approximation for the wind-turbine blades[1]. LES has the ability to simulate the flow through wind farms, where the turbulence is anisotropic and dominated by large scale structures and turbulent mixing.

With the use of LES in mind, we investigate an existing high-order symmetry-preserving finite-volume discretization of the Navier-Stokes equations on a staggered grid[2], based on the original second-order method of Harlow and Welch[3]. In such a symmetry-preserving discretization, sometimes called mimetic, the difference operators mimic the properties of the underlying differential operators. In this way not only mass and momentum are conserved, but also kinetic energy, a critical property for accurate LES[4,5,6], in particular in wind-turbine wake aerodynamics. The use of a high-order method prevents interference between the sub-grid scale model and truncation errors[7].

An ongoing problem in the use of high-order symmetry preserving discretizations is the prescription of boundary conditions which retain the formal order of accuracy of the discretization while respecting symmetry properties. In literature two different approaches can be identified:

- The construction of discretization schemes at the boundary with a *local* truncation error of order p. When having a stable discretization, this is a sufficient (but not necessary) condition to obtain p-th order accuracy of the global error[8]. This approach is followed for example by Hyman and Shashkov[9] and more recently by Castillo and others[10,11] (based on earlier work on mimetic discretizations by Hyman et al.[12,13], Castillo et al.[14] and Shashkov[15]), applying it mainly to diffusion problems with varying coefficients and non-smooth grids.
  In Castillo et al.[10] the important proposition is made that no mimetic discretization at Dirichlet boundaries exists that has a local truncation error which is better than first order when the standard inner product is employed. Discretizations with a higher-order local truncation error are therefore constructed with respect to an adapted inner product; symmetry properties are preserved with respect to this inner product.

- The construction of schemes which satisfy symmetry properties with respect to the standard inner product. Although this implies that the local truncation error cannot

be higher than first order, as mentioned above, it might not necessarily prevent the *global* error from reaching higher order. An example is the classical scheme of Harlow and Welch[3], which is symmetry-preserving and globally second-order accurate. The extension of this scheme to fourth order by Morinishi et al.[16] and Verstappen and Veldman[2] shows that even fourth-order global accuracy can be achieved.

The latter approach has the advantage that the standard inner product can be employed, leading to a natural definition of and bound for the kinetic energy of the flow. This prevents the use of schemes with complicated coefficients[9,10]. However, it is unclear yet how the global error can reach higher order when the local error is at most first order at the boundary. In this paper we will investigate the relation between local and global truncation error in detail and we will derive limits for the global truncation error for the fourth-order symmetry-preserving scheme of Verstappen and Veldman[2].

The outline of this paper is as follows. In section 2 the fourth-order symmetry-preserving discretization and boundary condition treatment is discussed. For this discretization a local and global error analysis is performed in section 3. Subsequently, in section 4 numerical experiments on the 1D convection-diffusion equation and 2D incompressible Navier-Stokes equations are carried out to strengthen the theoretical error analysis.

2 FOURTH-ORDER SYMMETRY-PRESERVING DISCRETIZATION

2.1 Governing equation

In order to investigate the effect of boundary conditions on local and global order behavior, we consider the linear convection-diffusion equation as a special case of the Navier-Stokes equations in one dimension:

$$c\frac{\mathrm{d}u}{\mathrm{d}x} = \nu\frac{\mathrm{d}^2u}{\mathrm{d}x^2}, \quad 0 \leq x \leq 1, \quad c < 0, \quad \nu > 0, \tag{1}$$

where c is the convecting velocity (equal to -1 in all cases), u the convected velocity and ν the viscosity coefficient. To study the effect of no-slip conditions, equation (1) is supplemented with Dirichlet boundary conditions:

$$u(0) = u_L, \quad u(1) = u_R, \tag{2}$$

which will be taken equal to 0 and 1, respectively. In operator notation equation (1) can be concisely written as

$$Lu = f, \tag{3}$$

where

$$L \equiv c\frac{\mathrm{d}}{\mathrm{d}x} - \nu\frac{\mathrm{d}^2}{\mathrm{d}x^2}, \quad f = 0. \tag{4}$$

For small values of ν a boundary layer develops at $x = 0$. Defining $\varepsilon = \nu/c$ ($\varepsilon < 0$), the exact solution to equation (1) is given by

$$u(x) = u_L + (u_R - u_L)\frac{e^{x/\varepsilon} - 1}{e^{1/\varepsilon} - 1}. \tag{5}$$

2.2 Symmetry properties

The convective and diffusive part of L have certain properties which we want to be mimicked by their discrete counterparts. These properties can be obtained following the approach outlined in Hyman et al.[9]. Assuming that a sufficiently smooth function ϕ exists with $\phi(0) = u_L$ and $\phi(1) = u_R$, we can construct a function $\tilde{u} = u - \phi$ that satisfies zero Dirichlet boundary conditions. The convection-diffusion equation for $\tilde{u}$ becomes:

$$c\frac{\mathrm{d}\tilde{u}}{\mathrm{d}x} - \nu\frac{\mathrm{d}^2\tilde{u}}{\mathrm{d}x^2} = \tilde{f}, \tag{6}$$

where $\tilde{f} = -c\frac{\mathrm{d}\phi}{\mathrm{d}x} + \nu\frac{\mathrm{d}^2\phi}{\mathrm{d}x^2}$ and $\tilde{u}(0) = \tilde{u}(1) = 0$. The solution $\tilde{u}$ lies in the space of scalar functions that are zero on the boundary Γ,

$$H^0 = \{v(x) \in H \mid v_\Gamma = 0\}, \tag{7}$$

with the following inner product:

$$(u, v)_{H^0} = \int_V uv \,\mathrm{d}V. \tag{8}$$

The properties of the convective operator are found by integrating the convective operator with a test function v,

$$\int_V \frac{\mathrm{d}\tilde{u}}{\mathrm{d}x} v \,\mathrm{d}x = [\tilde{u}v]_0^1 - \int_V \frac{\mathrm{d}v}{\mathrm{d}x}\tilde{u} \,\mathrm{d}x, \tag{9}$$

reducing to

$$\int_V \frac{\mathrm{d}\tilde{u}}{\mathrm{d}x} v \,\mathrm{d}x = -\int_V \frac{\mathrm{d}v}{\mathrm{d}x}\tilde{u} \,\mathrm{d}x, \tag{10}$$

for scalar functions in H^0. In terms of the inner product and the convective operator $C = \frac{\mathrm{d}}{\mathrm{d}x}$ this can be written as

$$(C\tilde{u}, v)_{H^0} = -(\tilde{u}, Cv)_{H^0}, \tag{11}$$

showing that C is a skew-symmetric operator: $C = -C^*$ (* denotes the adjoint). A similar analysis for the diffusive operator leads to

$$\int_V \frac{\mathrm{d}^2\tilde{u}}{\mathrm{d}x^2} v \,\mathrm{d}x = \int_V \tilde{u}\frac{\mathrm{d}^2 v}{\mathrm{d}x^2} \,\mathrm{d}x, \tag{12}$$

so

$$(D\tilde{u}, v)_{H^0} = (\tilde{u}, Dv)_{H^0}. \tag{13}$$

This shows that $D = \frac{\mathrm{d}^2}{\mathrm{d}x^2}$ is a symmetric operator: $D = D^*$.

2.3 Symmetry-preserving discretization interior

We apply a non-uniform vertex-centered finite-volume discretization to equation (1). A finite-volume discretization is a logical choice, not only because it is conservative, but also because the aforementioned symmetry properties are defined in terms of integrals. Anticipating Navier-Stokes simulations on Cartesian grids in two and three dimensions, we employ a fourth-order discretization that is constructed as a combination of two second-order discretizations, one on a fine and one on a coarse (staggered) grid[2,16] (see figure 1). This gives the following discretization for the convective term:

$$\Omega_i (C_h u_h)_i = \alpha \left(\frac{u_{i+1} - u_{i-1}}{2} \right) - \left(\frac{u_{i+3} - u_{i-3}}{2} \right), \tag{14}$$

where the effective finite volume size is given by

$$\Omega_i = \alpha \frac{h_i + h_{i+1}}{2} - \frac{h_{i-2} + h_{i-1} + h_i + h_{i+1} + h_{i+2} + h_{i+3}}{2}. \tag{15}$$

The subscript h denotes the discrete approximation to its continuous counterpart. When taking $\alpha = 27$ the local truncation error is fourth-order accurate. The discretization of the diffusive term is obtained by recognizing that the second-order derivative $\frac{\mathrm{d}^2}{\mathrm{d}x^2}$ can be written as an 'inner' derivative acting on an 'outer' derivative, or equivalently, a divergence operator acting on a gradient operator[14,15]. In fact, the divergence and gradient operators are each others negative adjoints, and this property is used to build the discretization scheme[a]. The gradient operator is defined at the staggered locations, and is formed as:

$$(G_h u_h)_{i+1/2} = \alpha \left(u_{i+1} - u_i \right) - \left(u_{i+2} - u_{i-1} \right). \tag{16}$$

The diffusive discretization then follows as

$$\Omega_i (D_h u_h)_i = (-G_h^* \Lambda^{-1} G_h u_h)_i, \tag{17}$$

where $\Lambda_{i+1/2} = \alpha h_{i+1} - (h_i + h_{i+1} + h_{i+2})$. This discretization preserves the symmetry of the differential operator. Note that the diffusive discretization reduces to the following stencil on uniform grids ($\alpha = 27$):

$$24h (D_h u_h)_i = \frac{u_{i-3} - 54u_{i-2} + 783u_{i-1} - 1460u_i + 783u_{i+1} - 54u_{i+2} + u_{i+3}}{24h}, \tag{18}$$

which is also reported in, for example, Castillo et al.[14] and Kampanis et al.[17].

[a]We note that this approach is also crucial for problems with varying viscosity coefficients, such as encountered in RANS and LES models that employ the Boussinesq hypothesis.

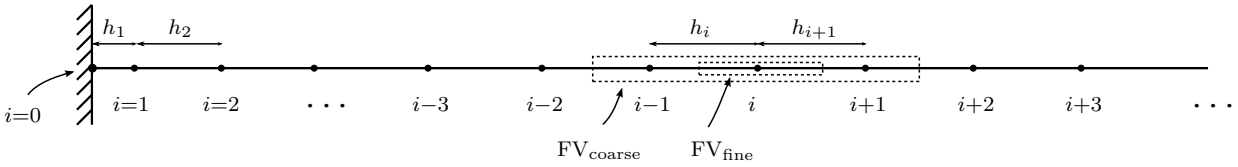

Figure 1: Vertex-centered discretization on non-uniform grid with fine and coarse finite volumes.

2.4 Symmetry-preserving discretization boundaries

Without loss of generality we consider the discretization at the left boundary (where the boundary layer is located). The points $i = 1$, 2 and 3 require the imposition of boundary conditions at the ghost points $i = -2$,-1 and 0. At $i = 0$ we have

$$u_0 = u_L. \tag{19}$$

At $i = -1$ one can use the Dirichlet condition at $i = 0$ to write

$$u_{-1} = 2u_L - u_1, . \tag{20}$$

Similarly, at $i = -2$ the following condition can be written:

$$u_{-2} = 2u_L - u_2, \tag{21}$$

but this condition only leads to the correct properties for the diffusive operator. For a skew-symmetric convection operator the boundary condition has to be chosen as

$$u_{-2} = u_2. \tag{22}$$

2.5 Resulting scheme

The resulting scheme is written as follows:

$$L_h u_h = f_h, \tag{23}$$

where

$$L_h = c\, C_h - \nu\, D_h, \tag{24}$$

and

$$f_h = -c\, f_h^c + \nu\, f_h^d. \tag{25}$$

The upper-left corner of the convective part reads

$$C_h = \frac{1}{2}\begin{bmatrix} 0 & \alpha+1 & 0 & -1 & & \\ -\alpha-1 & 0 & \alpha & 0 & -1 & \\ 0 & -\alpha & 0 & \alpha & 0 & \ddots \\ 1 & 0 & -\alpha & 0 & \alpha & \\ & \ddots & & \ddots & & \ddots \end{bmatrix}, \quad f_h^c = \frac{u_L}{2}\begin{bmatrix} -\alpha \\ 2 \\ 1 \\ 0 \\ \vdots \end{bmatrix}. \tag{26}$$

In a discrete setting the skew-symmetry property can be interpreted as follows: the contribution of a point $i+k$ to the derivative in point i is the negative of the contribution of point i to the derivative in point $i+k$. The diffusive part reads

$$D_h = \frac{1}{24h}\begin{bmatrix} -2\alpha^2+2\alpha-2 & \alpha^2+2\alpha-1 & -2\alpha & 1 & & \\ \alpha^2+2\alpha-1 & -2\alpha^2-2 & \alpha^2+2\alpha & -2\alpha & 1 & \\ -2\alpha & \alpha^2+2\alpha & -2\alpha^2-2 & \alpha^2+2\alpha & -2\alpha & \ddots \\ 1 & -2\alpha & \alpha^2+2\alpha & -2\alpha^2-2 & \alpha^2+2\alpha & \\ & \ddots & & \ddots & & \ddots \end{bmatrix}, \quad (27)$$

$$f_h^d = \frac{u_L}{24h}\begin{bmatrix} \alpha^2-2\alpha+2 \\ -2\alpha+2 \\ 1 \\ 0 \\ \vdots \end{bmatrix}. \quad (28)$$

The discretization at the right boundary is done in a similar fashion. The resulting matrix L_h is non-singular, leading to a *stable* discretization; in unsteady problems this provides a bound for the energy of the flow.

3 LOCAL AND GLOBAL ERROR ANALYSIS

The local truncation error is defined as

$$\tau \equiv L_h u - f_h. \quad (29)$$

Note that strictly speaking a restriction operator is necessary to map the continuous function u to the space of discrete functions to be able to apply L_h. The global error is defined as

$$e \equiv u - u_h, \quad (30)$$

which is related to τ as

$$L_h e = \tau. \quad (31)$$

3.1 Local truncation error

First we discuss the local truncation error of the convective terms on a uniform grid. The local truncation error is found by employing a Taylor series expansion for the exact solution u around a point x_i:

$$u(x_i+h) = u(x_i) + hu_i^{(1)} + \frac{1}{2}h^2 u_i^{(2)} + \mathcal{O}(h^3), \quad (32)$$

where $u_i^{(n)} = \left(\frac{\mathrm{d}^n u}{\mathrm{d}x^n}\right)_i$. Applying operator C_h we find:

$$\tau_i^c = -\frac{9}{5}h^5 u_i^{(5)} + \mathcal{O}(h^7). \quad (33)$$

The truncation error is fifth order instead of fourth order because we work in a finite volume setting. To find τ at $i = 1$ and 2, where the stencil changes due to boundary conditions, we employ a Taylor expansion for u_L:

$$u_L = u_1 - hu_1^{(1)} + \frac{1}{2}h^2 u_1^{(2)} + \mathcal{O}(h^3). \tag{34}$$

This leads to the following truncation errors:

$$\tau_1^c = 2hu_1^{(1)} - 2h^2 u_1^{(2)} + \mathcal{O}(h^3), \tag{35}$$

$$\tau_2^c = -\frac{1}{2}h^2 u_2^{(2)} + \mathcal{O}(h^3). \tag{36}$$

It turns out that the convective discretization at $i = 1$ is *inconsistent*. Considering boundary condition (22) this is not a surprise, although one should recall that also standard second-order schemes are inconsistent at boundaries[18].

The same procedure is followed to analyse the truncation error of the diffusive terms:

$$\tau_i^d = -\frac{9}{40}h^5 u_i^{(6)} + \mathcal{O}(h^7), \tag{37}$$

$$\tau_1^d = \frac{25}{12}hu_1^{(2)} - \frac{25}{12}h^2 u_1^{(3)} + \mathcal{O}(h^3), \tag{38}$$

$$\tau_2^d = -\frac{1}{24}hu_2^{(2)} + \frac{1}{12}h^2 u_2^{(3)} + \mathcal{O}(h^3). \tag{39}$$

The diffusive discretization is inconsistent at both $i = 1$ and $i = 2$.

3.2 Global truncation error

Although the discretization at the boundaries is inconsistent, it is still possible to obtain convergence of the global error. In order to show this we use the approach outlined in Wesseling[18] for second-order schemes. Recall the relation between the global and local truncation error, equation (31):

$$L_h e = \tau. \tag{40}$$

We assume that L_h is a monotone operator, i.e.

$$L_h v \geq 0 \quad \text{implies} \quad v \geq 0. \tag{41}$$

Equivalently one can say that L_h is monotone iff $L_h^{-1} \geq 0$ [b]. If we can construct a function E, a so-called *barrier function*, such that[c]

$$L_h E \geq |\tau|, \tag{42}$$

[b] $a \geq 0$ means that $a_i \geq 0 \; \forall \, i$; $A \geq 0$ means that $A_{ij} \geq 0 \; \forall \, i, j$

[c] $|a|$ is the vector with elements $|a_i|$

then, subtracting this equation from (40), we obtain

$$L_h(e - E) \leq 0. \tag{43}$$

Since L_h is assumed monotone, this means that

$$e - E \leq 0 \quad \rightarrow \quad e \leq E. \tag{44}$$

The art is to construct a barrier function E of a certain order p such that (42) holds, since this will prove that the global error e is also of order p. Since any sufficiently differentiable continuous function can be expressed as a polynomial expansion, we take $E = h^p\psi(x)$ with

$$\psi(x) = a_0 + a_1 x + a_2 x^2 + a_3 x^3 + a_4 x^4. \tag{45}$$

It is possible to include more terms in this expansion, but later on it will turn out that this is not necessary.

Note that proving monotonicity of L_h for the fourth-order discretization is not trivial. Normally, monotonicity can be proven by showing that L_h is positive[d]. For second-order central discretizations positivity is proven when the mesh Péclet number h/ν is smaller than 2. For the fourth-order scheme this approach fails, because L_h can never be positive, as can be observed by inspecting the signs of the diagonals of $c\,C_h - \nu D_h$. However, a non-positive operator can still be monotone (see for example Lorenz[19] and Axelsson and Kolotilina[20]). We have not yet found a sufficient condition for monotonicity of the fourth-order scheme, but at this stage it suffices to say that we have found, by explicitly computing L_h^{-1}, that L_h is monotone if h/ν is small enough.

3.2.1 Interior

In a general interior point i we can write for L_hE:

$$L_h(h^p\psi(x))_i = 24h^{p+1}\left(c\,(4a_4x_i^3 + 3a_3x_i^2 + 2a_2x_i + a_1) - \nu(12a_4x_i^2 + 6a_3x_i + 2a_2)\right). \tag{46}$$

We recognize the exact first and second derivatives of $\psi(x)$. This is because τ_i^c and τ_i^d only contain derivatives of fifth order and higher: L_h can differentiate a fourth-order polynomial *exactly*. Of course we can take more terms in expansion (45); these will not be exactly differentiated. Since τ_i is

$$\tau_i = c\,\tau_i^c - \nu\tau_i^d = -c\,\frac{9}{5}h^5u_i^{(5)} + \nu\frac{9}{40}h^5u_i^{(6)} + \mathcal{O}(h^7), \tag{47}$$

we find that $L_hE - |\tau|$ can be written as

$$\begin{aligned} L_hE_i - |\tau_i| = {} & 24\,h^{p+1}\left(c\,(4a_4x_i^3 + 3a_3x_i^2 + 2a_2x_i + a_1) - \nu(12a_4x_i^2 + 6a_3x_i + 2a_2)\right) \\ & - h^5\left|-c\frac{9}{5}u_i^{(5)} + \nu\frac{9}{40}u_i^{(6)}\right| + \mathcal{O}(h^7). \end{aligned} \tag{48}$$

[d]positivity implies monotonicity, but not vice versa

For $p \leq 4$ it is possible to construct the coefficients a_n such that $L_h E - |\tau| \geq 0$. This indicates that a fourth-order accurate local truncation error leads to a fourth-order accurate global error, as expected.

3.2.2 Boundary, $i = 1$

The analysis is now repeated for the boundary points. At $i = 1$ ($x_1 = h$) the local error is

$$\tau_1 = c\,\tau_1^c - \nu\tau_1^d = c\,2hu_1^{(1)} - \nu\frac{25}{12}hu_1^{(2)} - c\,2h^2u_1^{(2)} + \nu\frac{25}{12}h^2u_1^{(3)} + \mathcal{O}(h^3), \tag{49}$$

so we obtain

$$L_h(h^p\psi(x))_1 - |\tau_1| = h^p\left(c\,\frac{27}{2}a_0 + \nu\frac{677}{24h}a_0 + \mathcal{O}(h)\right) - h\left|c\,2u_1^{(1)} - \nu\frac{25}{12}u_1^{(2)} + \mathcal{O}(h)\right|. \tag{50}$$

To make sure that the order of the first term does not exceed the order of the truncation error (for $h \to 0$), we require $p \leq 2$. For example, in case $p = 2$, the leading order term condition is

$$h\left(\frac{677}{24}\nu a_0 - \left|c\,2u_1^{(1)} - \nu\frac{25}{12}u_1^{(2)}\right|\right) \geq 0. \tag{51}$$

This means that with a sufficiently large positive value of a_0 (depending on c and ν) we have found a barrier function that is always larger than $|\tau|$ for sufficiently small h. Only the first term of the polynomial expansion (45) is of importance here; increasing the polynomial order will not change equation (51). *With a polynomial as barrier function it is not possible to demonstrate a convergence rate higher than 2 in the limit* $h \to 0$. Considering the fact that any sufficiently differentiable function on the domain $x \in [0, 1]$ can be expressed as a polynomial, it seems plausible that *no barrier function exists with which we can prove a convergence rate higher than 2.* To complete the proof for $p = 2$, we have to check if the polynomial barrier function can also dominate the local truncation error at $i = 2$.

3.2.3 Boundary, $i = 2$

At $i = 2$ ($x_2 = 2h$), we have

$$\tau_2 = c\,\tau_2^c - \nu\tau_2^d = \nu\frac{1}{24}hu_2^{(2)} - c\,\frac{1}{2}h^2u_2^{(2)} - \nu\frac{1}{12}h^2u_2^{(3)} + \mathcal{O}(h^3), \tag{52}$$

and we obtain

$$L_h(h^p\psi(x))_2 - |\tau_2| = h^p\left(-c\,a_0 - \nu\frac{13}{6h}a_0\right) - h\left|\nu\frac{1}{24}u_2^{(2)} + \mathcal{O}(h)\right|. \tag{53}$$

This indicates again that the maximum order of the global error is $p = 2$ if the following condition can be fulfilled:

$$h\left(-\frac{13}{6}\nu a_0 - \left|\nu\frac{1}{24}u_2^{(2)} + \mathcal{O}(h)\right|\right) \geq 0. \tag{54}$$

However, this requires $a_0 < 0$, which contradicts the requirement for $i = 1$. For the current boundary layer problem we can escape from this by noting that $\tau_1 > 0$, $\tau_2 < 0$ and $|\tau_1| > |\tau_2|$. This means that the absolute value signs are too restrictive; a range of positive values of a_0 exists for which both (51) and (54) are satisfied.
Nevertheless, for more general problems without exact solution (e.g., 2D, non-linear, with source terms) the signs of τ_1 and τ_2 are not known a priori and second order can possibly not be proven.

4 NUMERICAL EXPERIMENTS

4.1 1D convection-diffusion equation

4.1.1 Uniform grid

First we validate the fourth-order scheme by using 'exact' boundary conditions, i.e. we substitute the exact solution (5) for the ghost points, like in Veldman[21]. For $\nu = 1/100$ and $h = 1/200$ ($|h/\varepsilon| = 1/2$) the discrete and exact solution are shown in figure 2(a). The global truncation error $e = u - u_h$ and local truncation error, obtained from $\tau = L_h e$, are shown in figure 2(b). The leading error term of the theoretical local truncation error, equation (47), is found by using the exact solution, equation (5):

$$\tau_i = \left(-\frac{9}{5} + \frac{9}{40}\right)\left(\frac{h}{\varepsilon}\right)^5 \frac{e^{x_i/\varepsilon}}{e^{1/\varepsilon} - 1}, \tag{55}$$

and is also shown in figure 2(b). Because equation (55) contains only the leading error term, there is a small deviation between the two local truncation errors. The local truncation error always attains its maximum (in absolute sense) at $i = 1$, because $e^{x/\varepsilon}$ is largest here (note $\varepsilon < 0$). The global error, on the other hand, does not necessarily attain its maximum value in the first grid point: this depends on L_h^{-1}. The structure of L_h^{-1} is shown in figure 2(c); all entries are ≥ 0, so L_h is indeed monotone in this case. It can be seen that L_h^{-1} distributes the local error τ over the entire domain in a particular way. For instance, e_1 is influenced by τ in the entire domain, whereas e_N is mainly influenced by τ at the right side of the domain. This is because the 'flow' is convection-dominated and information travels from right to left ($c < 0$).

A plot of $\|e\|$ as a function of h displays a clear fourth-order convergence in both the L_2 and the L_∞ norms, see figure 2(d). The local error $\|\tau\|$ shows fifth-order convergence, as expected from (55).

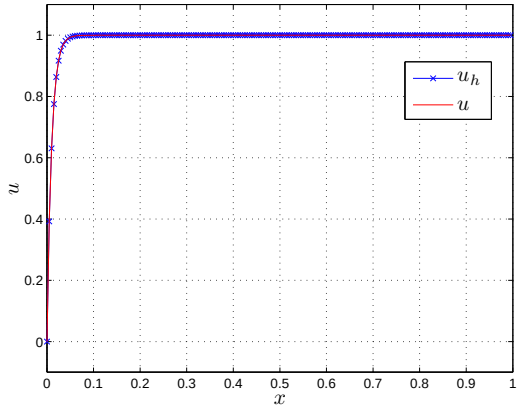

(a) Discrete and exact solution, $h = 1/200$.

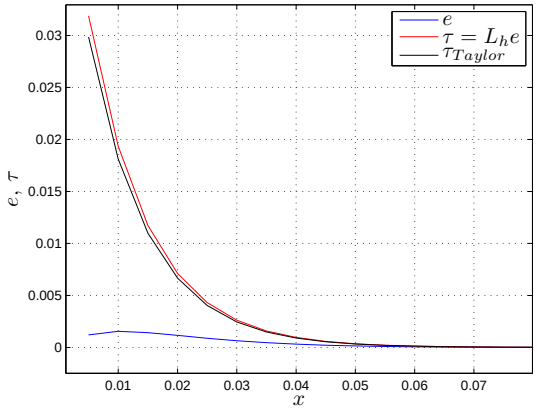

(b) Global and local truncation error, $h = 1/200$.

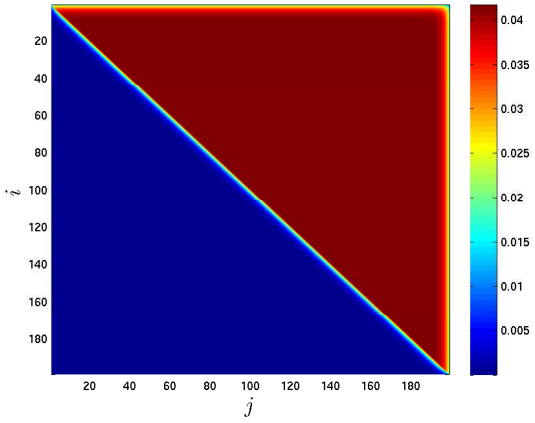

(c) Structure of L_h^{-1}, $h = 1/200$.

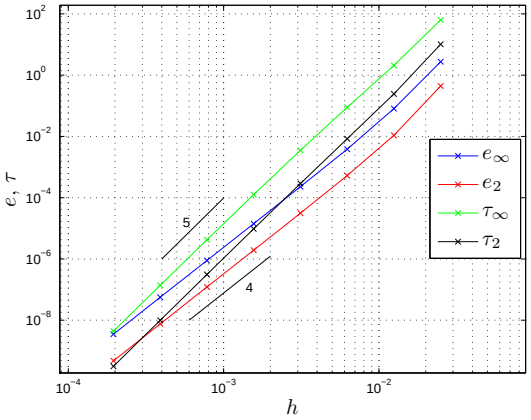

(d) Convergence of global error.

Figure 2: Solution and error behavior for uniform grid, exact boundary conditions, $\nu = 1/100$.

Now we turn to the results for scheme (23)-(28) where the boundary conditions are chosen such that symmetry properties of the discrete operators are retained. Figure 3(a) shows that the behavior of the local truncation error near the boundary is much more irregular, as expected. As predicted by equations (49) and (52), the convergence of the local error at the boundary is first order for sufficiently small h. The global error shows second-order convergence, confirming the barrier function analysis from section 3.2. Note that numerical experiments showed that (at $\nu = 1/100$) L_h is monotone for $h < 1/60$, approximately. In the L_2 norm the global error converges with third order, showing that the second-order behavior is very local and is averaged out in the L_2 norm.

A closer inspection of figure 3(b) shows that some 'kinks' are apparent in the convergence of global and local error. A better understanding of these kinks is obtained when looking at the position of maximum local and global error, figure 3(c):

- The location of the maximum local truncation error is either at $i = 1$ or $i = 2$. This location can in principle be found a priori from Taylor expansions, but only when the exact solution is known. When the location changes, $\|\tau\|_\infty$ shows small kinks, in $\|\tau\|_2$ these changes are smoother.
- The location of the global error is either at $i = 1$, 2 or 3. This is not only depending on the behavior of τ, but also on the behavior of L_h^{-1}. At the point where the position of the global error changes from $i = 3$ to $i = 1$, $\|e\|_\infty$ shows a kink ($h \approx 2 \cdot 10^{-4}$). The rate of convergence of the global error depends therefore on the position of the maximum error.

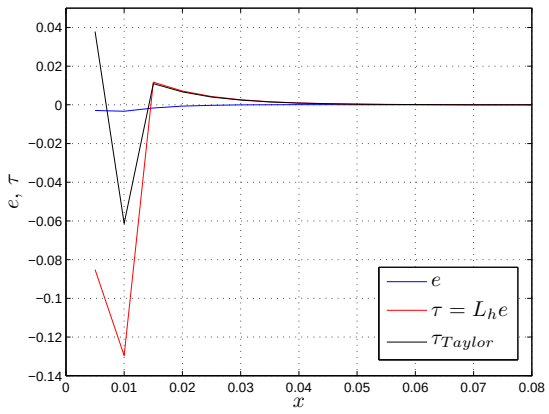

(a) Global and local truncation error, $h = 1/200$.

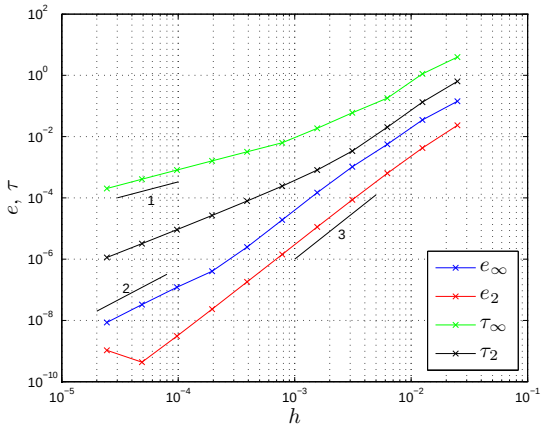

(b) Convergence of global and local error.

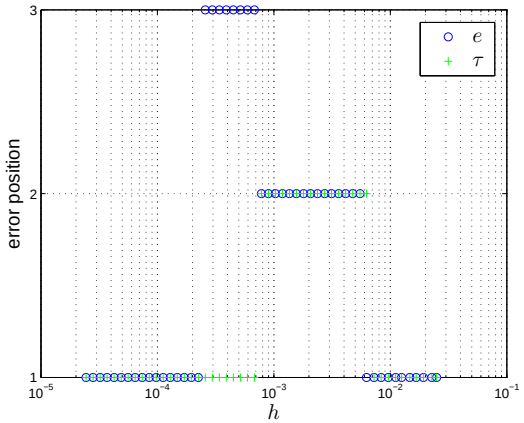

(c) Position of maximum global and local error.

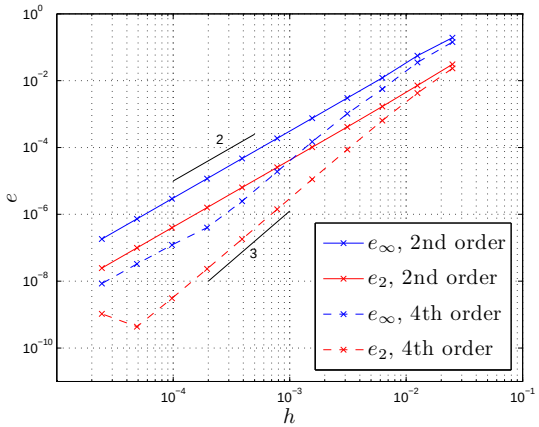

(d) Comparison of second- and fourth- order scheme.

Figure 3: Error behavior for uniform grid, symmetry-preserving boundary conditions, $\nu = 1/100$.

Considering that both theoretical arguments and numerical experiments show that

the fourth-order symmetry-preserving method is only second-order accurate for boundary layer problems with Dirichlet boundary conditions, one might wonder if it is useful to apply a fourth-order method anyway. We therefore compare the results presented above with those of a standard second-order method, which does not require boundary conditions for u_{-1} and u_{-2}. The global error behavior of the second- and fourth-order schemes is shown in figure 3(d). It is observed that the global error for the fourth-order scheme is smaller than the global error for the second-order scheme for all meshes considered here, in both norms.

We remark that for smaller ν (thinner boundary layers) the kink in the global error (where it is positioned at $i = 1$) is at a *smaller* h, giving a larger region of 'almost third order' convergence.

4.1.2 Non-uniform grid

In practice, thin boundary layers are calculated by employing non-uniform grids. In this section we investigate if the conclusions for uniform grids carry over to non-uniform grids. First we investigate an exponential grid, i.e. a grid where each cell size is a constant factor times the neighboring grid cell size. The grid is written as a mapping of a uniform grid,

$$x(\xi) = (1 - s^{\xi})/(1 - s), \tag{56}$$

where ξ is uniformly distributed over $[0, 1]$, and s is the stretch factor. The stretch factor is determined by choosing a refinement region δ such that in both $[0, \delta]$ and $[\delta, 1]$ $N/2$ volumes are located. Defining the boundary layer edge as the point where $u = p\,u_R$, we find for sufficiently small ε:

$$\delta_p = \varepsilon \ln(1 - p). \tag{57}$$

For example, if the boundary layer edge is defined at the point where $u = 0.99$, then $\delta_{0.99} \approx 4.6 \cdot 10^{-2}$ ($\varepsilon = -1/100$). In figure 4(a) we have plotted u as a function of ξ for different values of p. It can be seen that for smaller p the gradient of $u(\xi)$ at the left boundary becomes smaller. Looking at the convergence and position of the local and global error for $\delta_{0.99}$ (figures 4(b) and 4(c)) it can be seen that the refinement region can make sure that the position of maximum global error is not at the boundary. However, for sufficiently small h it is again observed that the global error moves to the boundary, and the slope changes to second order ($h \approx 5 \cdot 10^{-3}$). For smaller p this change occurs at a lower value of h. The value of ν influences the position of this kink in a similar way; for strongly convection-dominated flows one might not notice the change to second order!

Comparing the global error of the fourth-order scheme with the standard second-order scheme, it is observed that (for the meshes considered here) the fourth-order scheme is always more accurate than its second-order counterpart, as was the case on uniform grids. Because of the rapid fourth-order convergence at coarse meshes the error of the fourth-order scheme is already 100 times smaller at $h = 10^{-2}$. Thus, *the fourth-order scheme is attractive on non-uniform meshes.* However, for a good comparison with the second-order

scheme we need to take into account computational time, so that we can evaluate the time needed by both methods to reach a desired accuracy. Such an evaluation is preferably to be done in 2D or 3D.

A subtlety of the exponential meshes just discussed is that upon refinement the stretch factor of the mesh is kept constant, meaning that not every cell is exactly halved. We therefore investigated two other types of meshes as well:

- Exponential meshes which are formed by starting from a very fine exponential mesh and then constructing a coarse mesh by removing every second grid line. In this way the stretch factor is different for each grid. It turns out that the error behavior is almost identical to the exponential meshes discussed above.

- Shishkin meshes (see e.g.[18]), consisting of two uniform meshes with a different mesh width. The point where the mesh changes is taken equal to δ, defined before. It turns out that also on Shishkin meshes the error behavior for the fourth-order scheme is second order. The position of largest error is always around the Shishkin point, where the mesh size changes abruptly. Although the error is in the interior, fourth-order accuracy is not reached due to the lack of smoothness of the grid. Recalling that the relation between the derivative on a uniform and non-uniform grid is given by

$$\frac{\mathrm{d}u}{\mathrm{d}x} = \frac{\mathrm{d}u}{\mathrm{d}\xi} \Big/ \frac{\mathrm{d}x}{\mathrm{d}\xi}, \tag{58}$$

  we observe that an $\mathcal{O}(h^4)$ approximation for both $\frac{\mathrm{d}u}{\mathrm{d}\xi}$ and $\frac{\mathrm{d}x}{\mathrm{d}\xi}$ is required, which is not the case for Shishkin meshes.

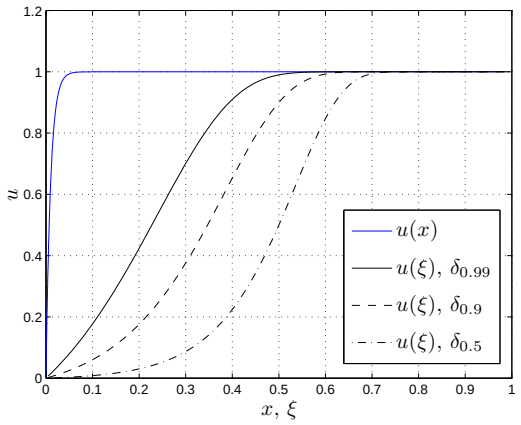

(a) Discrete solution $u(x)$ and $u(\xi)$, $h = 1/200$.

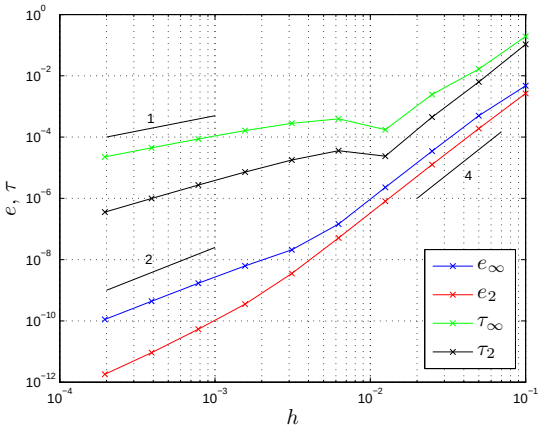

(b) Convergence of global and local error, $\delta_{0.99}$.

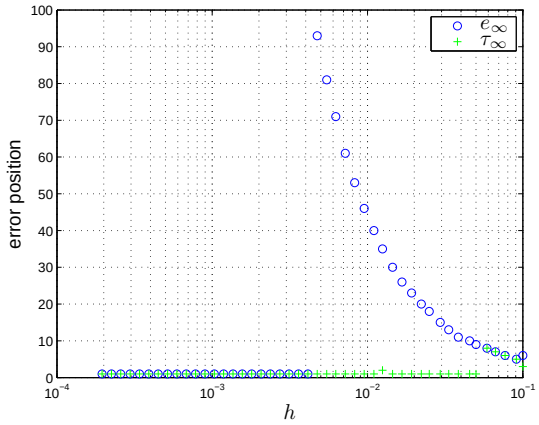

(c) Position of maximum global and local error, $\delta_{0.99}$.

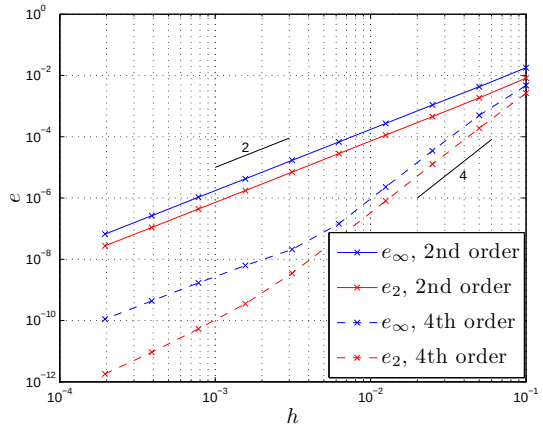

(d) Convergence of global error, second- and fourth-order scheme, $\delta_{0.99}$.

Figure 4: Solution and error behavior for non-uniform grid, $\nu = 1/100$.

4.2 2D lid-driven cavity

To investigate the order behavior of the fourth-order scheme with symmetry-preserving Dirichlet boundary conditions, a mesh convergence study of the steady lid-driven cavity flow at a Reynolds number of 1000 is performed. In this benchmark problem[22,23] for the incompressible Navier-Stokes equations (NS) we introduce two major differences with the 1D convection-diffusion equation: (i) NS are non-linear, (ii) NS include a pressure term to satisfy the incompressibility constraint. The extension from 1D to 2D is straightforward, with the exception that the convecting velocity c requires other boundary conditions than the convected velocity u (momentum), for details see[2]. We look for steady solutions, so the full non-linear system of equations is solved with Newton linearization of the convective term. The resulting saddle-point matrix is solved with a direct solver in Matlab. The iterative procedure is stopped when the residual (in the maximum norm) drops below 10^{-12}, which requires approximately 10 iterations.

To investigate mesh convergence as a function of the number of finite volumes we consider the global kinetic energy of the flow in the cavity. Bruneau and Saad[22] report a value of 0.44503, obtained on a uniform grid having 1024^2 volumes. A more accurate estimate is obtained by a Richardson extrapolation incorporating values from their 256^2 and 512^2 grids, resulting in a value of $k^* = 0.0445189$. This value is used here to evaluate the error: $e = |k - k^*|$, where $k = \frac{1}{2}(u_h, \Omega u_h)$.

Figure 5(a) shows the error as a function of the mesh size for five different grid types: uniform, exponential (with the aforementioned mesh parameter $\delta = 0.01$, 0.05 and 0.1) and cosine ($x = \frac{1}{2}(1 - \cos(\pi\xi))$). We note the following:

- On uniform grids the fourth-order discretization is only more accurate than its second-order counterpart on very coarse grids. Upon grid refinement the second-order scheme shows second-order behavior, but the fourth-order scheme shows first-order behavior. This confirms the doubts expressed in section 3.2 which indicated that proving second-order behavior for problems more general than the 1D convection-diffusion equation might not succeed.

- On cosine grids the second- and fourth-order discretization both behave as second order, but the fourth-order one has a smaller error constant. The error behavior is very regular.

- On exponential grids we observe a rapid error decrease on coarse grids; the fourth-order scheme is approximately an order of magnitude more accurate than the second-order scheme. However, the fourth-order scheme displays first-order behavior on fine meshes, and the second-order scheme becomes more accurate (like for uniform grids).

Figure 5(b) shows the error as a function of the CPU time. Although we should take into account that currently the system is solved with the direct solver of Matlab (probably not the most efficient method to solve the saddle-point system), this figure is in principle

of much practical interest when choosing a method. For this test case we can say that the second-order scheme is to be preferred over the fourth-order scheme, but for coarse meshes there are regions where the fourth-order scheme can be more efficient (in terms of CPU time / error).

In order to exclude a possible influence of the singularities in the upper corners of the cavity on the error convergence (making Taylor expansions invalid), we have repeated the calculations for the regularized cavity problem[22], where the velocity of the lid is given by $u(x) = 16x^2(1-x)^2$. The resulting error behavior (not shown here) is very similar to the standard cavity problem, with two noticeable differences: the error for the regularized problem is in general smaller, and the error behavior for the fourth-order scheme is smoother at coarse grids.

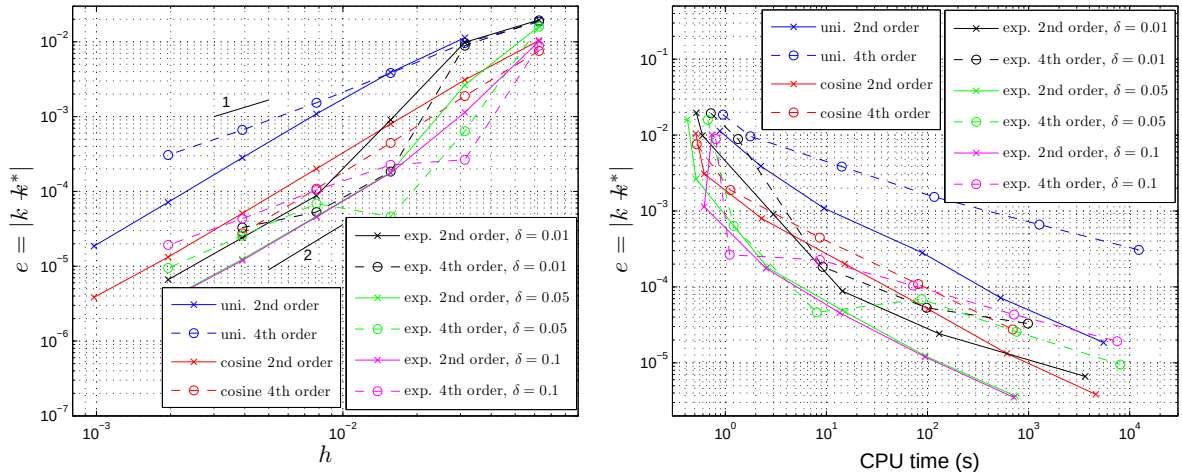

(a) as a function of the average mesh width.

(b) as a function of the CPU time.

Figure 5: Error in kinetic energy; uni.=uniform, exp.=exponential.

5 CONCLUSIONS

In this paper we have investigated the local and global error behavior of a fourth-order symmetry-preserving scheme for flows involving boundary layers. It turns out that, although the local truncation error is inconsistent, this does not hold for the global error. In fact, numerical experiments supported with theoretical arguments showed that the global error of the fourth-order scheme is limited to second order in case of Dirichlet boundary conditions. On properly chosen exponential grids fourth-order convergence behavior seems to be obtained for coarse meshes, but for finer meshes the convergence rate drops back to second order. Further analysis showed that this drop is directly related to the location where the maximum error occurs.

In two-dimensional simulations of the lid-driven cavity similar behavior was observed.

The fourth-order scheme with Dirichlet boundary conditions is at most second order (cosine grids), but can even be first order (uniform grids). Only at coarse grids the fourth-order scheme is markedly better than its second-order counterpart. With these observations we re-interpret the fourth-order method of Verstappen and Veldman[2] in the following way: when Dirichlet boundaries are involved, the method is at maximum second order in the infinity norm, but with a suitably chosen non-uniform grid a region of fourth-order convergence can appear.

In practical simulations, the fourth-order scheme might still be of interest. Firstly, in LES coarse grids are the rule and fine grids the exception. Furthermore, for external flows Dirichlet boundary conditions are in general less influential than in the currently simulated internal flow. We have only looked at the kinetic energy of the flow to test convergence and not at more physically relevant results like velocity profiles. Lastly, preserving symmetry properties has been found to be crucial for unsteady turbulence simulations, whereas the current simulations are still steady and laminar. In any case, the current work provides a background which should be taken into account when using symmetry-preserving schemes with symmetry-preserving boundary conditions.

References

[1] B. Sanderse, S.P. van der Pijl, and B. Koren. Review of CFD for wind-turbine wake aerodynamics. *Submitted to Wind Energy*.

[2] R.W.C.P. Verstappen and A.E.P. Veldman. Symmetry-preserving discretization of turbulent flow. *J. Comput. Phys.*, 187:343–368, 2003.

[3] F.H. Harlow and J.E. Welch. Numerical calculation of time-dependent viscous incompressible flow of fluid with free surface. *Phys. Fluids*, 8:2182–9, 1965.

[4] K. Mahesh, G. Constantinescu, and P. Moin. A numerical method for large-eddy simulation in complex geometries. *J. Comput. Phys.*, 197:215–240, 2004.

[5] R. Mittal and P. Moin. Suitability of upwind-biased finite difference schemes for large-eddy simulation of turbulent flows. *AIAA J.*, 35(8), 1997.

[6] B. Perot. Conservation properties of unstructured staggered mesh schemes. *J. Comput. Phys.*, 159:58–89, 2000.

[7] A.G. Kravchenko and P. Moin. On the effect of numerical errors in large eddy simulations of turbulent flows. *J. Comput. Phys.*, 131:310–322, 1997.

[8] T.A. Manteuffel and A.B. White. The numerical solution of second-order boundary value problems on non-uniform meshes. *Math. Comput.*, 47(176):511–535, 1986.

[9] J.M. Hyman and M. Shashkov. Approximation of boundary conditions for mimetic finite-difference methods. *Comp. Math. Appl.*, 36(5):79–99, 1998.

[10] J.E. Castillo and R.D. Grone. A matrix analysis approach to higher-order approximations for divergence and gradients satisfying a global conservation law. *SIAM J. Matrix. Anal. A.*, 25(1):128–142, 2003.

[11] O. Montilla, C. Cadenas, and J. Castillo. Matrix approach to mimetic discretizations for differential operators on non-uniform grids. *Math. Comput. Simulat.*, 73:215–225, 2006.

[12] J.M. Hyman, R.J. Knapp, and J.C. Scovel. High order finite volume approximations of differential operators. *Physica D*, 60:112–138, 1992.

[13] J. Hyman, M. Shashkov, and S. Steinberg. The numerical solution of diffusion problems in strongly heterogeneous non-isotropic materials. *J. Comput. Phys.*, 132:130–148, 1997.

[14] J.E. Castillo, J.M. Hyman, M.J. Shashkov, and S. Steinberg. The sensitivity and accuracy of fourth order finite-difference schemes on nonuniform grids in one dimension. *Comp. Math. Appl.*, 30(8):41–55, 1995.

[15] M. Shashkov. *Conservative Finite-Difference Methods on General Grids*. CRC Press, 1996.

[16] Y. Morinishi, T.S. Lund, O.V. Vasilyev, and P. Moin. Fully conservative higher order finite difference schemes for incompressible flows. *J. Comput. Phys.*, 143:90–124, 1998.

[17] N.A. Kampanis and J.A. Ekaterinaris. A staggered, high-order accurate method for the incompressible Navier-Stokes equations. *J. Comput. Phys.*, 215:589–613, 2006.

[18] P. Wesseling. *Principles of Computational Fluid Dynamics*. Springer, 2001.

[19] J. Lorenz. Zur Inversmonotonie diskreter Probleme. *Numer. Math.*, 27:227–238, 1977.

[20] O. Axelsson and L. Kolotilina. Monotonicity and discretization error estimates. *SIAM J. Numer. Anal.*, 27(6):1591–1611, 1990.

[21] A.E.P. Veldman. High-order symmetry-preserving discretization of convection-diffusion equations on strongly stretched grids. In *Int. Conf. on Boundary and Interior Layers*, 2006.

[22] C.-H. Bruneau and M. Saad. The 2D lid-driven cavity problem revisited. *Comput. Fluids*, 35:326–348, 2006.

[23] O. Botella and R. Peyret. Benchmark spectral results on the lid-driven cavity flow. *Comput. Fluids*, 27(4):421–433, 1998.